Pergamon

Bioorganic & Medicinal Chemsitry, Vol. 2, No. 4, pp. 279-296, 1994

0968-0896/94 $7.00 + .00

0968-0896(94)E0010-Y

Synthesis, Molecular Modelling, and NMR Structure Determination of four Cyclic Peptide Antagonists of Endothelin

Erin K. Bradley,* Simon C. Ng, Reyna J. Simon and David C. Spellmeyer
Chiron Corporation, 4560 Horton Street, Emeryville, CA 94608, U.S.A.

Abstract—A combined distance geometry and molecular mechanics/dynamics (MM/MD) protocol was unable to predict the active conformation of the cyclic pentapeptide inhibitor of endothelin-1 receptor, BQ-123, and two analogues. However, the MM/MD method alone is sufficient to predict the solution conformation of a third analogue. In that one case, the combination of proline at residue 3 and an N^{α}-methyl substitution at residue 5 provides enough internal constraints to eliminate conformational flexibility seen in the other three analogues. For this constrained analogue, the 50 lowest energy conformations (out of a set of 500 DGEOM-generated, MM/MD minimized conformations) differ by no more than 3.9 kcal/mol. Thirty three of these 50 conformations have backbone atom RMSDs of less than 0.33 Å, relative to the lowest energy conformation. The accuracy of this MM/MD model is verified by determining the solution structure of each of the four analogues with 2D NMR techniques. Each of the cyclic pentapeptides has a well defined solution conformation where a proline residue is clearly in a γ-turn, leaving the remaining residues in a loose β-turn. All four experimental NMR conformations agree closely with the MM/MD model.

Introduction

Computational and structural biochemists face a difficult challenge: the 3D structure of a bound conformation of a potent ligand must be solved or predicted in a timely manner for any conformation-based inhibitor design project to be useful in lead optimization. We will demonstrate that the solution conformation of a potent endothelin receptor ligand can be predicted rapidly with a judicious choice of computational method. Preliminary NMR information allowed us to eliminate the conformations of three closely related peptides from consideration as potential models for conformation-based inhibitor design approaches. We have since solved the NMR conformation of all four endothelin receptor ligands, validating our original choice of model.

An intensely competitive effort to discover novel antagonists to the two known receptor subtypes of the most potent endogenous vasoconstrictor known, endothelin-1 (ET-1),[1] has developed since ET-1 was discovered in 1988. One receptor subtype, designated ETR_A, is involved in vasoconstriction,[2] while the other, designated ETR_B, is implicated in both vasoconstriction and vasodilation.[3] Several ligands to the ETR_A and/or the ETR_B subtypes have been reported recently, representing several different chemical classes.[4–20] We chose to develop models and to solve the NMR solution conformation for a closely related series of cyclic pentapeptide inhibitors of the ETR_A receptor reported in 1991.[4–6] To improve our understanding of the bound conformation of these cyclic peptides, we synthesized, determined the binding affinities, and solved the solution conformation of two closely related peptides initially not reported. The solution conformation of these compounds is very similar to those reported for the parent compound, BQ-123[21–23] and another closely related analogue, BE18257B.[24]

Here we report our efforts to determine the conformation of BQ-123 (compound **1** see Table 1) and three analogues using molecular mechanics and dynamics (MM/MD) simulations, and to verify those models using 2-dimensional nuclear magnetic resonance (2D NMR). Our

Abbreviations—Dtrp D-tryptophan, Dphe D-phenylalanine, Dtyr D-tyrosine, Dasp D-aspartic acid, Dval D-valine, Nmleu Nα-methyl-L-leucine, ET-1 endothelin 1.
MM/MD molecular mechanics/molecular dynamics, DG distance geometry, RMS root mean square, RMSD root mean square deviation.
NMR nuclear magnetic resonance, 2D NMR 2-dimensional NMR, ROESY 2-dimensional rotating frame nuclear Overhauser effect spectroscopy, COSY 2-dimensional J-correlated spectroscopy, PECOSY 2-dimensional exclusive correlation spectroscopy, TOCSY 2-dimensional total correlation spectroscopy, $^3J_{N\alpha}$, NH-C^{α}H vicinal proton coupling constant, $^3J_{\alpha\beta}$ C^{α}H-C^{β}H vicinal proton coupling constant.
FMOC 9-(fluorenylmethoxy)carbonyl, PyBOP benzotriazole-1-yl-oxy-tris-(pyrrolidino)phosphonium hexafluorophosphate, PyBrOP, bromo-tris-(pyrrolidino)phosphonium hexafluorophosphate, HOBt hydroxybenzotriazole, DMSO dimethyl sulfoxide, DCM dichloromethane, DMF dimethyl formamide, DIEA diisopropylethanolamine, TFA trifluoroacetic acid, EtOH ethanol, HOAc acetic acid, TMS tetramethylsilane, DMAP dimethylaminopyridine, DIC diisopropylcarbodiimide.
RP-HPLC reverse phase high pressure liquid chromotography, AAA amino acid analysis, FAB-MS fast atom bombardment mass spectral analysis.
We use the designations ETR_A and ETR_B, rather than the convention ET_A and ET_B to ensure clarity that we are discussing the two receptor subtypes of the Endothelin family.

initial studies using MM/MD methods alone enabled us to predict the solution conformation of one of these analogues, compound **4**, (Nmleu,[5] see Table 1). We were unable to predict the solution conformation of the other analogues due to the presence of multiple low-energy conformers. The accuracy of our model of compound **4** has been verified by the agreement of all four experimental NMR conformations with the predicted MM/MD conformation.

Results and Discussion

Peptide synthesis and characterization

The peptides used in this study were prepared by one of two similar routes, shown in Figure 13. The linear protected precursors were synthesized using 9-(fluorenylmethoxy)carbonyl (FMOC) protected amino acids with PyBOP [benzotriazole-1-yl-oxy-tris-(pyrrolidino)-phosphonium hexafluorophosphate] and HOBt (hydroxy-benzotriazole) activation[25] except in the case of Nα-methyl leucine (Nmleu) which was coupled using PyBrOP [bromo-tris-(pyrrolidino)phosphonium hexafluorophosphate] activation.[26] Cyclization was accomplished in solution with the linear protected precursors using PyBOP and HOBT.[25] The reactions were monitored by analytical HPLC. Intermediate products were not purified. In each case, the desired product was the major component observed in the chromatography, although higher oligomers may not have been seen under these conditions. Following cyclization and Dasp sidechain deprotection, the peptides were purified to homogeneity on C_{18} reversed phase high pressure liquid chromatography (RP-HPLC). Amino acid analysis and mass spectral analysis were performed prior to NMR studies.

Receptor binding affinity.

Receptor binding assays for ETR_A were performed using murine 3T3 cells as described previously.[14] These results are listed in Table 1 along with binding data on ETR_A and ETR_B reported by Ishikawa and co-workers for BQ-123 and compound **4** (Nmleu[5]).[6]

Molecular mechanics/molecular dynamics without NMR constraints

We observed no significant conformational preference in our molecular modeling studies on the first reported cyclic pentapeptide antagonist, BE18257B, (compound **5**),[4] despite the constraint of cyclization. The range of energies for the 20 lowest energy conformations is only 10 kcal/mol and the root-mean-square deviation (RMSD) of the backbone atoms from the lowest energy conformation is 2.3 Å. The sidechains are clearly not constrained in these calculations. Figure 1 shows the 10 lowest energy conformations with the backbone atoms superimposed. These gas-phase results are not well enough constrained to be useful in a 3D conformation-based design approach.

Further computational work on this compound proved unnecessary when subsequent compounds were reported which had more internal constraints than compound **5**.[5–6] We then concentrated our modeling efforts on two of the newer compounds (**1** and **4**) as well as two other compounds (**2** and **3**). Compound **4** (Nmleu[5]) looked especially promising because it appeared to be strongly constrained by the combination of the Pro in position 3 and the Nmleu in position 5.

Indeed, compound **4** is a well constrained molecule. We find that the 50 lowest energy conformations out of a set of 500 distance geometry-generated, MM/MD minimized conformations differ by no more than 3.9 kcal/mol. Of these 50 conformations, 33 have backbone atom RMSDs less than 0.33 Å, relative to the lowest energy conformation, regardless of the distance geometry method used (see 'Materials and Methods' section for details of the calculations). Figure 2 shows this low energy conformation and the superposition of the 20 lowest energy conformers from the distance geometry–dynamics run. This peptide shows a γ-turn centered around the proline and a loose β-turn with Leu–Dtrp at the i+1 and i+2 residues. This agrees with preliminary NMR studies reported for BQ-123 (compound **1** in this study).[21–23]

Table 1. Peptide sequences* and binding cosntants.

Compound		Position					IC50 (uM)		
Name	#	1	2	3	4	5	ETR_A‡	ETR_A∞	ETR_B**
BQ-123†	**1**	Dtrp	Dasp	Pro	Dval	Leu	0.0017	0.022	18
Dtyr[1]	**2**	**Dtyr**	Dasp	Pro	Dval	Leu	0.67		
Dphe[1]	**3**	**Dphe**	Dasp	Pro	Dval	Leu	0.23		
Nmleu[5]	**4**	Dtrp	Dasp	Pro	Dval	**Nmleu**	0.0020	0.035	>100
BE18257B§	**5**	Dtrp	Dglu	Ala	**D-*allo*-Ile**	Leu			

*All peptides are cyclized in a head-to-tail manner.
†Ishikawa *et al.*[5,6]
§Ihara *et al.*[4]
‡Mouse 3T3 cells as described in Spellmeyer *et al.*[14]
∞Reported by Ishikawa *et al.*[6] for porcine aortic smooth muscle.
**Reported by Ishikawa *et al.*[6] for porcine cerebellum membranes.

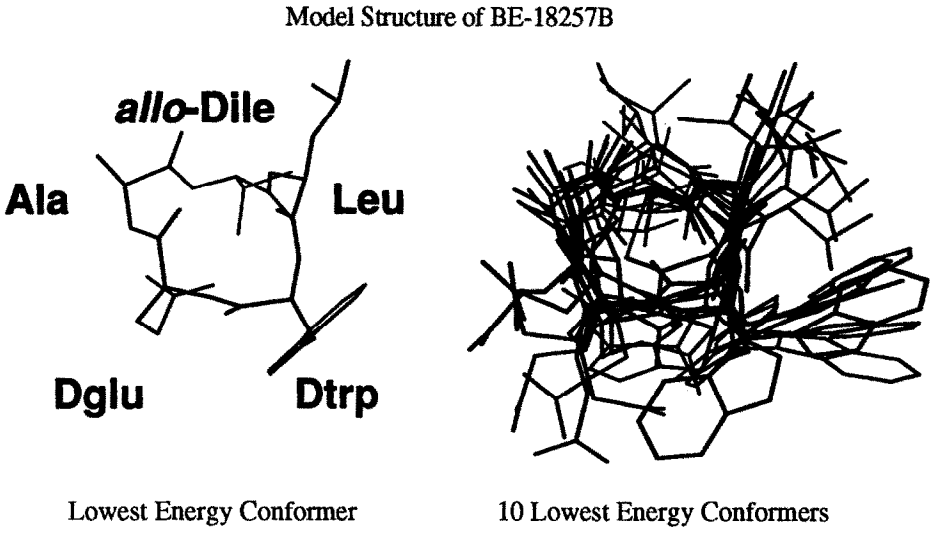

Figure 1. Compound **5**, (Left) The lowest energy conformer from a combined distance geometry and molecular mechanics/dynamics simulation; (Right) the 10 lowest energy conformers from the same simulation, with backbones (N, CA, C, O) superimposed. The average mainchain RMSD is 1.18 Å. Note: this peptide appears to have no conformational preference.

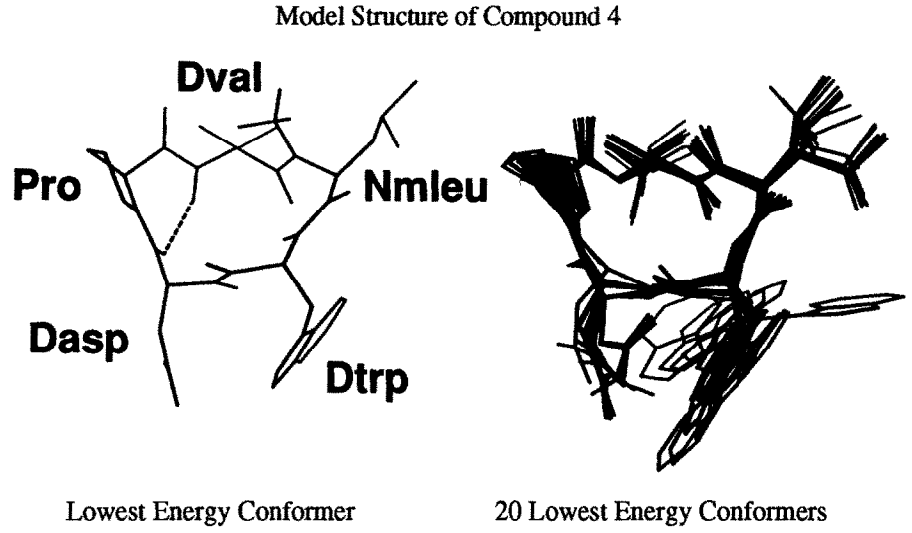

Figure 2. Compound **4** [Nmleu^5], (Left) The lowest energy conformer from a combined distance geometry and molecular mechanics/dynamics simulation; (Right) the 20 lowest energy conformers from same simulation, with backbones (N, CA, C, O) superimposed. The average mainchain RMSD is 0.34 Å. Note: this peptide shows definite conformational preference, with a γ-turn centered at Pro and a β-turn over the rest of the residues.

The α carbons all lie approximately in one plane. Although the backbone atoms are well constrained, the sidechains exhibit more variability, except for Pro 3. This proline residue probably locks the peptide into the preferred γ and β-turns. The Dval sidechain lies largely in the same plane as the peptide backbone and shows rotations about the Cα–Cβ bond in which the two methyl groups point either to the Nmleu residue or to the underside (as seen in Figure 2) of the peptide backbone ring. The Nmleu sidechain also occupies an area of space that is largely in the plane of the peptide backbone. Here, all the accessible sidechain conformations are sampled, suggesting they are not limited by the bulky methyl group at the N nor by the Dtrp sidechain. Likewise, the Dtrp sidechain samples many possible rotamers, populating a large area of space under the peptide backbone ring, as viewed with the N to C direction aligned in a clockwise manner. The Dasp sidechain populates all possible rotamers, but seems to have two distinct preferred conformations, placing the acid moiety 'under' the ring on the face opposite to the proline sidechain.

The theoretical model of compound **1** (BQ-123) is more constrained than that of compound **4**, regardless of the distance geometry method used to generate the initial conformations. We expected the opposite, since the absence of the N^{α}-methyl group on the leucine should have removed steric hindrance internal to the ring. The 50 lowest energy conformations span 3.6 kcal/mol and the maximum backbone RMS deviation is 0.3 Å, relative to the lowest energy conformation. All 50 of these have two γ-turns, one centered on the Pro and the other on the Dval residue, see Figure 3. In addition, the sidechain conformations are more well defined than those described

above for compound **4**. These conformations are extremely well converged. However, our NMR results and those from literature reports[21–23] show this to be an unrealistic conformation in solution. Elimination of these anomalous low-energy conformations leaves us with structures that show neither backbone nor sidechain conformational preference.

This double γ-turn is not an artifact of the distance geometry method employed, since similar results are obtained regardless of the variant of distance–geometry used to generate the initial starting conformations. In each of the sets generated with one of the four distance geometry methods, almost 250 conformations of the 500 initial conformers show this double γ-turn.

This double γ-turn is also not a result of the choice of dielectric constant (ε=4r) used for our MM/MD calculations. A weaker dielectric constant (ε=16r) should damp out the charge–charge interactions and decrease the number of conformations with the anomalous γ-turns. Calculations with this weaker dielectric constant provide nearly identical results. It is possible that simulations with full solvent would not exhibit this tendency to form a double γ-turn.

Thus, this double γ-turn seems to be a consequence of the well-defined γ-turn at the proline, enhanced relative to a linear peptide through the cyclic constraints and conformational restriction of the proline residue. Replacement of the N^{α}-methyl group with the proton creates an N–H group juxtaposed to H-bond with the carbonyl of the proline. Since the AMBER force-field overestimates the stability of γ-turns in gas-phase calculations,[27] conformers with a second γ-turn at the Dval residue are stabilized relative to those without the second γ-turn.

Compound **3** ($Dphe^{1}$) also shows a tendency to converge to a conformation with a double γ-turn, Figure 4. These conformations are nearly identical to those discussed for compound **1** (BQ-123). They have highly similar backbone conformations and the sidechains populate few of the possible alternatives. We believe the presence of a double γ-turn in this conformation is also anomalous. Removal of the conformations with these double γ-turns left conformations with no well-defined backbone or sidechain conformation.

We were concerned that the conformational convergence of these models to the double γ-turn form was the result of poor sampling during initial distance geometry structure generation. In order to increase the diversity of initial conformations, we generated starting conformations for compound **2** ($Dtyr^{1}$) in which all the peptide bonds were allowed to randomly sample between *cis* and *trans*. Since the AMBER force-field has been parameterized with *trans* amide bonds lower in energy than *cis*, any *cis* peptide bonds (expect for proline) were expected to flip back to *trans* during the simulations.

Combining all four of the distance geometry runs for compound **2**, the 50 lowest energy conformations spanned 5.8 kcal/mol and the maximum backbone RMS deviation is 2.1 Å, relative to the lowest energy conformation. However, many of the lowest energy conformations contain *cis* peptide bonds between non-proline residues. This theoretical result contradicts experimental NMR evidence—obtained after the simulations were complete—that no *cis* peptide bonds exist in this molecule. Subsequently, we learned that anomalous *cis* peptide bonds have been observed as the low-energy conformations of other cyclic peptides when modeled with the AMBER force-field.[28] AMBER apparently underestimates the energy of the *cis* peptide bond in the case of cyclic peptides. Therefore, we believe that any conformation of this molecule containing a *cis* peptide bond is invalid.

Removal of those conformations with the *cis* peptide bonds leaves conformations that contain the double γ-turn seen in compounds **1** and **3**. Likewise, NMR evidence shows that these double γ-turn conformations are not present in solution. Figure 5 shows the 20 lowest energy conformations of compound **2**.

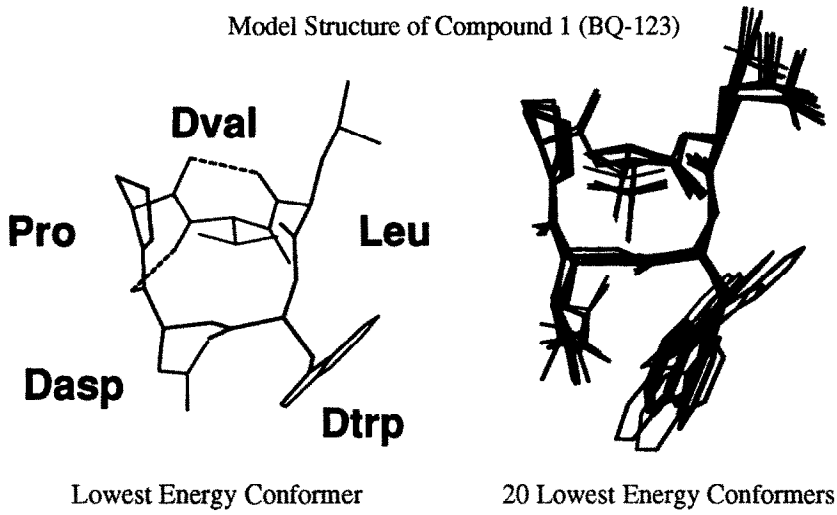

Figure 3. Compound **1** [BQ-123], (Left) The lowest energy conformer from a combined distance geometry and molecular mechanics/dynamics simulation; (Right) the 20 lowest energy conformers from same simulation, with backbones (N, CA, C, O) superimposed. The average mainchain RMSD is 0.47 Å. Note: these conformers are extremely well converged in the anomalous double γ-turn motif.

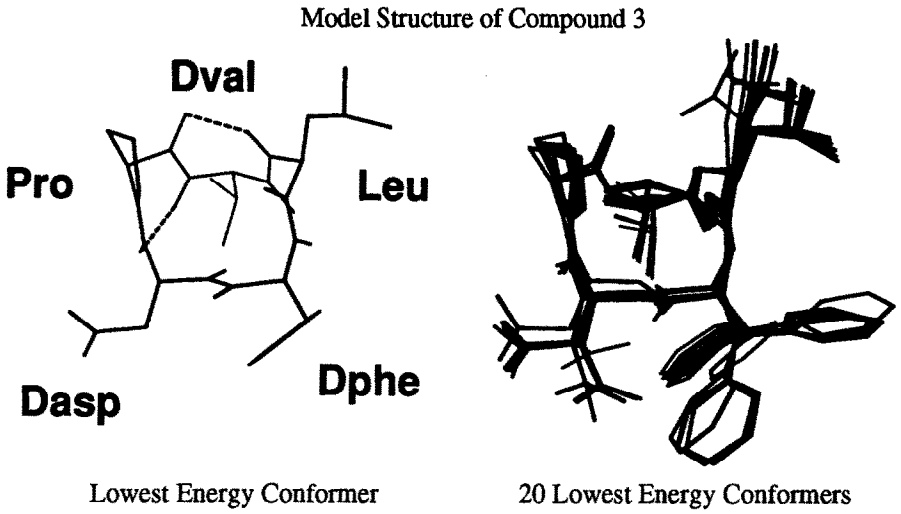

Figure 4. Compound **3** [Dphe[1]], (Left) The lowest energy conformer from a combined distance geometry and molecular mechanics/dynamics simulation; (Right) the 20 lowest energy conformers from same simulation, with backbones (N, CA, C, O) superimposed. The average mainchain RMSD is 0.37 Å. Note: these conformers are also extremely well converged in the anomalous double γ-turn motif.

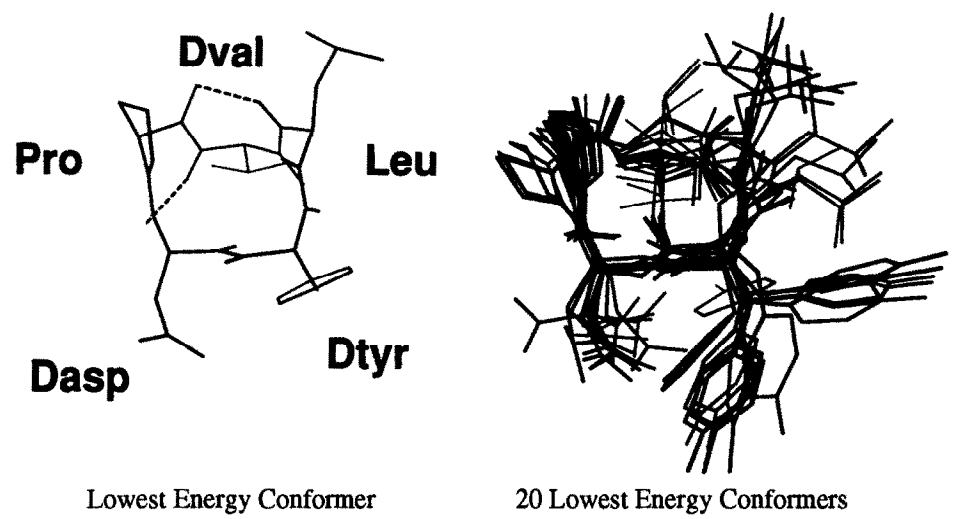

Figure 5. Compound **2** [Dtyr[1]], (Left) The lowest energy conformer from a combined distance geometry and molecular mechanics/dynamics simulation; (Right) the 20 lowest energy conformers from same simulation, with backbones (N, CA, C, O) superimposed. The average mainchain RMSD is 1.04 Å. Note: this peptide does not appear to have as strong a conformational preference as compound **4**.

In the end, with one of the four analogues (Nmleu[5]) and some preliminary NMR information, we have developed a model useful for further work. This conformational model has two N-substituted residues within the cyclic pentapeptide backbone, which provide enough steric interaction to lock the backbone into one predominant conformation. The N^{α}-methyl group on the leucine also prohibits formation of a γ-turn at the Dval residue. The results from this simulation are in contrast to the simulations of the other analogues. Once conformations known to be in error are removed from consideration, the simulated conformations of the other analogues are poorly converged, and are thus not useful models.

Nuclear magnetic resonance

The NMR spin system assignments of all the analogues were straightforward using methods described by Wüthrich.[29] The TOCSY[30] spectra for each analogue were easy to assign because each sidechain was unique. However, the sequential connections were slightly complicated because of significant overlaps between the NH/CαH crosspeaks seen in the ROESY[31,32] fingerprint region. This is shown for compound **2** (Dtyr[1]) in Figure 6. The ^{1}H assignments for each of the analogues are shown in Table 2.

The crosspeak overlap caused further difficulties, when important constraints were lost because the intra-residue crosspeak 5NH/CαH overlaps the inter-residue crosspeak between 5CαH/lNH in the ROESY spectra of both compounds **1** (BQ-123) and **2** (Dtyr[1]). An average of 30 conformationally relevant distance constraints were generated from the ROESY spectra for compounds **1–3**,

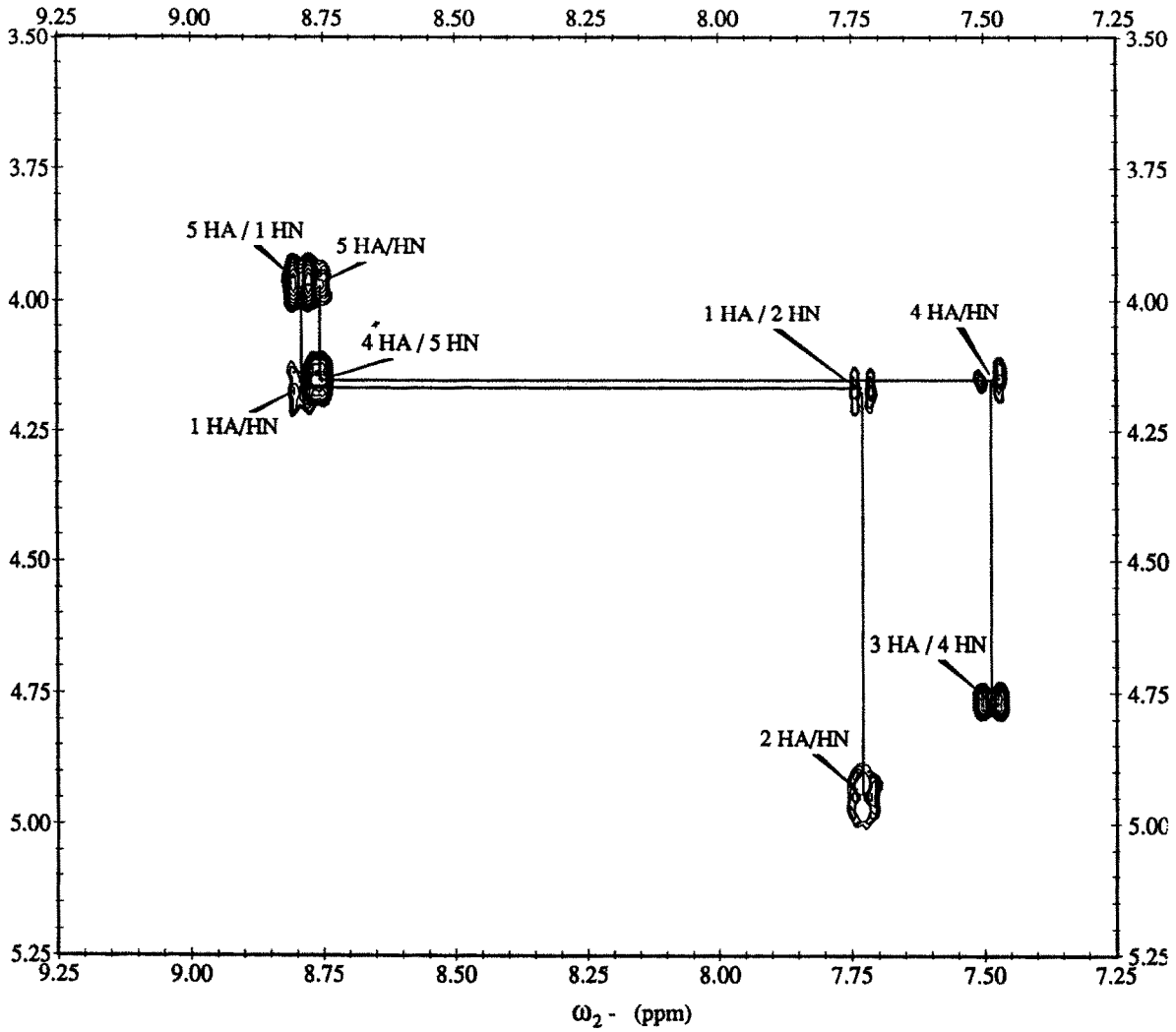

Figure 6. ROESY fingerprint region for compound **2** [Dtyr^1]. Spectra taken with a 200 ms mixing time at 30 °C in DMSO (d6). Crosspeak assignments and sequential connection are shown. Residue 3 is a Pro, which lacks an amide proton (NH), so there is no 3 HA/HN or 2 HA/3 HN crosspeak. Note: there are two pairs of overlapped crosspeaks near 8.7 ppm: 1 HA/HN overlaps 4 HA/5 HN, and 5 HA/HN overlaps 5 HA / 1 HN.

but only 21 were generated for compound **4** (Nmleu^5). A coincidence of the proton chemical shift for 4α and 5α, as well as 1β and 5 N$^\alpha$-methyl severely limited our ability to assign a number of crosspeak constraints unambiguously for Nmleu^5. The exact number of constraints is shown in Table 5, and the constraint files are available as supplemental material.

The $^3J_{N\alpha}$ coupling constants were used to generate constraints on the dihedral angles between the HN and Hα of each residue (see 'Materials and Methods' section for details of the calculations). The angular constraints are shown in Table 3. The $^3J_{\alpha\beta}$ coupling constants, determined from a PECOSY,[33] were used to make stereo-specific assignments, shown in Table 4 in the manner described by Basus.[34] Stereo-specific assignment of β-protons (indicated in Table 2) made distance constraints unambiguous for those protons. Thus there was no need to include pseudo atoms or replace the protons with heavy atom CB constraints in refinement.

One hundred conformations were generated and subjected to refinement as described in the 'Materials and Methods' section. After refinement, each conformation was considered to satisfy NMR constraints if it met these criteria:

- no NH/CαH dihedral angle constraint violations > 10°;
- no single distance constraint violation > 0.5 Å;
- no more than 2 distance constraint violations > 0.3 Å;
- no χ angle constraint violations of any size.

After initial refinement, we noticed a large number of final conformations were produced with a *cis* peptide bond between residues 5 and 1 in both compound **1** (BQ-123) and compound **2** (Dtyr^1). The presence of the 5CαH/1NH crosspeak in both the ROESY spectra indicates that there is no *cis*- peptide bond present. The presence of *cis* peptide bonds in the final conformations could be an artifact of imposing distance constraints on the AMBER potentials. However, this cannot be the sole reason, because no *cis* peptide bonds were observed after the refinement of compound **3** (Dphe^1). As noted previously both compounds **1** and **2** had overlapped 5NH/CαH and 5CαH/1NH crosspeaks, so these constraints were not included in the refinement. The missing 5CαH/1NH

Table 2. Proton resonance assignments† (DMSO, 30 °C).

	NH	αH	βH	γH	δH	other
BQ-123						
Dtrp	8.75	4.25	2.89§			δ1 7.13 ε1 10.76
			3.32§			ε3 7.50 η2 7.04
						ζ2 7.30 ζ3 6.95
Dasp	7.69	4.96	2.32§			
			2.79§			
Pro		4.75	1.60§	1.75	3.14	
			2.25§	1.90	3.30	
Dval	7.49	4.16	1.66	0.84		
				0.84		
Leu	8.73	3.98	1.16	1.00	0.60	
			1.16		0.72	
Dtyr¹						
Dtyr	8.79	4.16	2.59§			δ 7.02 ε 6.61
			3.11§			
Dasp	7.73	4.94	2.34§			
			2.80§			
Pro		4.77	1.60§	1.75	3.12	
			2.25§	1.90	3.29	
Dval	7.49	4.14	1.69	0.84		
				0.84		
Leu	8.75	3.96	1.15	0.99	0.65	
			1.25		0.75	
Dphe¹						
Dphe	8.90	4.26	2.70§			δ 7.25
			3.25§			
Dasp	7.78	4.95	2.37§			
			2.80§			
Pro		4.75	1.60§	1.75	3.11	
			2.25§	1.90	3.30	
Dval	7.50	4.15	1.68	0.85		
				0.85		
Leu	8.78	3.95	1.15	0.87	0.60	
			1.25		0.70	
Nmleu⁵						
Dtrp	8.41	4.33	2.90			δ1 7.11 ε1 10.78
			3.23			ε3 7.52 η2 7.02
						ζ2 7.30 ζ3 6.95
Dasp	7.64	4.87	2.38			
			2.82			
Pro		4.74	1.65	1.77	3.15	
			2.24	1.89	3.40	
Dval	7.58	4.49	1.85	0.83		
				0.89		
Nmleu		4.48	1.18	0.95	0.65	N^{α}-methyl 2.90
			1.34		0.76	

†Assignments were performed in the manner of Wutrich *et al.*[29] using double quantum phase-sensitive COSY[58,59], TOCSY[30], and ROESY[31,32].
§Stereo specifically assigned.

distance would have constrained the peptide bond between residues 5 and 1 to a *trans* conformation. We believe that this missing distance constraint contributed to this refinement error. Analogues that were missing this distance constraint in refinement had a large number of final conformations with *cis* peptide bonds. As mentioned earlier, the AMBER force-field has been observed to underestimate the energy of a *cis* peptide bond in cyclic peptides.[28] Thus we cannot expect the force-field to compensate for the missing NMR constraints, and it may even aggravate the problem.

In order to reduce the number of final conformations containing *cis* peptide bonds, another set of refinements was run using an increased force constant on the *cis / trans* interconversion of the peptide bond. When the peptide bond was constrained to its starting conformation by increasing the force constant, the presence of *cis* peptide bonds between residues 5 and 1 was eliminated. It is reassuring that the refinement results for compound **3** (Dphe¹), which never had *cis* peptide bonds, is basically unchanged when the higher force constant is used.

After the last set of refinements, each analogue had at least 20 converged conformations that met the criteria listed above. The final converged conformations are shown superimposed for compounds **1** through **4** in Figures 7–10, respectively. The centroid[35] from the final set of conformations for each analogue is shown superimposed on the predicted Nmleu⁵ analogue conformation, in Figure 11. The number of final conformations, the RMSDs between conformations, the maximum dihedral violations and maximum distance violations are shown in Table 5.

Table 3. $^3J_{N\alpha}$ Coupling constants and ϕ related dihedral constraints.

Residue		$^3J_{N\alpha}$* (Hz)	Theoretical Θ† (°)	Θ Constraint (°)
	1	8.30	**154/-154**	-145 to -165§
BQ-123	2	9.04	**162/-162**	-155 to 155
	4	10.01	**180**	-170 to 170
	5	5.13	**128/-128/34/-34**	120 to 140§
	1	8.46	**155/-155**	-145 to -165§
Dtyr[1]	2	8.87	**160/-160**	-155 to 155
	4	10.47	**180**	-170 to 170
	5	5.24	**129/-129/33/-33**	120 to 140§
	1	8.46	**155/-155**	-145 to -165§
Dphe[1]	2	8.87	**160/-160**	-155 to 155
	4	10.07	**180**	-170 to 170
	5	4.84	**125/-125/37/-37**	115 to 135§
	1	8.79	**159/-159**	-150 to 150
Nmleu[5]	2	8.79	**159/-159**	-150 to 150
	4	9.77	**180**	-170 to 170

*In DMSO at 30 °C.
†Calculated using the equation from Pardi *et al.*[63]: $^3J_{N\alpha} = 6.4\cos^2\Theta - 1.4\cos\Theta + 1.9$. Angluar values in bold print are included within the refinement constraints.
§Constraint range selected to meet structures without distance violations from an initial refinement run without this constraint.

The NMR conformation of compound **4** (Nmleu[5]) is not as well defined as the other analogues (Figure 10). We believe this is the result of fewer distance and angular constraints, 21 versus an average of 30 distances, and 3 versus 7 dihedral constraints. The smaller number of constraints is due to chemical shift overlap and lack of an amide proton in the Nmleu residue.

The theoretical MM/MD conformation of Nmleu[5] agrees well with the NMR conformations of all the analogues. The backbone RMSD between the theoretical conformation of compound **4** (Nmleu[5]) and the centroid of the final set of NMR conformations for compounds **1** (BQ-123), **2** (Dtyr[1]), **3** (Dphe[1]), and **4** (Nmleu[5]) are 0.35 Å, 0.45 Å, 0.33 Å, and 0.17 Å, respectively. In these conformations, the proline is clearly in a γ-turn, leaving the remaining residues in a loose β-turn. The carbonyls in the β-turn tend to point away from the middle of the ring, while the amide protons tend to point inward. This is consistent with other reported conformations of BQ-123 and BE18257B in the literature.[21–24] Table 6 shows a comparison of main chain dihedrals between our NMR conformations, our theoretical model, and those previously published for BQ-123 and BE18257B.

The theoretical conformations show many potential sidechain conformations are populated (Figure 2). In the models of Nmleu[5], the Dtrp sidechain is found in several conformations, all lying under the ring of the backbone There are two rotamers of the Dval and two of the Nmleu. In contrast, the NMR conformations have well defined sidechain conformations for residues 1 and 2, due to both distance and χ angle constraints. In all cases, the sidechains lie almost in the plane of the backbone atoms. This agrees with the conclusions of Atkinson and Pelton.[21]

Materials and Methods

Peptide synthesis, purification and characterization

The syntheses of compounds **1–3** started with commercially available FMOC–Leu–WANG resin.[44] Benzyl protection was used for the Dasp sidechain. Standard methods were used for synthesis and cleavage.[45] Specifically, for compound **1** the TFA cleavage solution was concentrated, lyophilized from acetic acid and used without further purification giving the linear protected peptide **1a** in > 80% purity. Cyclization was accomplished in a DMF solution of peptide at a concentration of approximately 1 mg/mL to minimize intermolecular reactions. PyBOP/HOBt/DIEA (2.5 eq/2.5 eq/5 eq) chemistry was used and the reaction appeared to be complete after 24 hours. The final step of debenzylation of the Dasp sidechain was easily accomplished by catalytic hydrogenation. Purified material was obtained following preparative C_{18} RP-HPLC. This protocol was also used in the preparation of compounds **2** and **3**.

The synthesis of compound **4** differed only slightly. Acid-labile Rink acid resin[46] was used for the preparation of the linear precursor, with *t*-butyl protection for the Dasp

Table 4. $^3J_{\alpha\beta}$ Coupling constants and χ related dihedral constraints.

	Proton†		$^3J_{\alpha\beta}$* (Hz)	Conformation‡	χ (°)	Constraint (°)
BQ-123	1	HB1	12.0	g^2t^3	60	20 to 100
		HB2	7.5			
	2	HB1	4.0	t^2g^3	180	-140 to 140
		HB2	10.0			
	3	*HB1*	8.0			
		HB2	<2.0			
	4	HB	7.0	free rotation§		
	5		overlap∞			
Dtyr¹	1	HB1	12.0	g^2t^3	60	20 to 100
		HB2	8.0			
	2	HB1	7.0	t^2g^3	180	-140 to 140
		HB2	11.0			
	3	*HB1*	7.0			
		HB2	<2.0			
	4	HB	7.0	free rotation§		
	5		overlap∞			
Dphe¹	1	HB1	13.0	g^2t^3	60	20 to 100
		HB2	7.5			
	2	HB1	5.0	t^2g^3	180	-140 to 140
		HB2	12.0			
	3	*HB1*	8.5			
		HB2	<2.0			
	4	HB	8.0	free rotation§		
	5		overlap∞			
Nmleu⁵	1	*HB1*	10.0			
		HB2	4.0			
	2	*HB1*	6.0			
		HB2	10.0			
	3	*HB1*	8.0			
		HB2	<2.0			
	4	HB	8.0	free rotation§		
	5	*HB1*	8.0			
		HB2	8.0			

*In DMSO at 30 °C.
†Assignments of protons made in the manner described by Basus[34] taking into account the presence of D-amino acids. Protons in *italics* are not stereo specifically assigned.
‡Assignments of conformation made in the manner described by Basus[34] taking into account the presence of D-amino acids.
§Measurement of $^3J_{\alpha\beta}$ for valine in this range are indicative of free rotation.[34]
∞The crosspeaks for HB1 and HB2 overlapped.

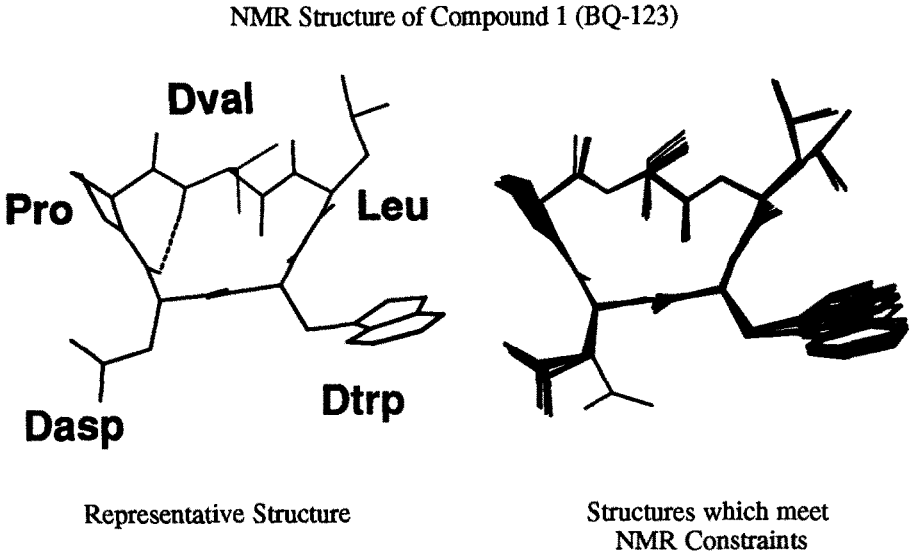

Figure 7. Compound 1 [BQ-123], (Right) the final 22 refined NMR structures, with backbones (N, CA, C, O) superimposed; (Left) the centroid[35] from the refined NMR structures. Note: In contrast to the DG/MD models, the sidechains are well constrained, especially the αβ-bond vector. The average mainchain RMSD between the final structures is 0.14 Å.

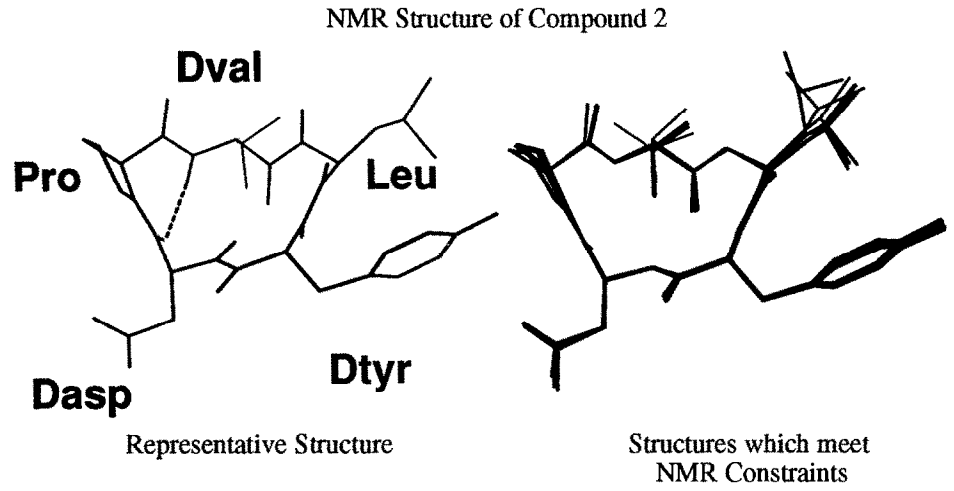

Figure 8. Compound **2** [Dtyr[1]], (Right) the final 36 refined NMR structures, with backbones (N, CA, C, O) superimposed; (Left) the centroid[35] from the refined NMR structures. Note: In contrast to the DG/MD models, the sidechains are well constrained, especially the αβ-bond vector. The average mainchain RMSD between the final structures is 0.08 Å.

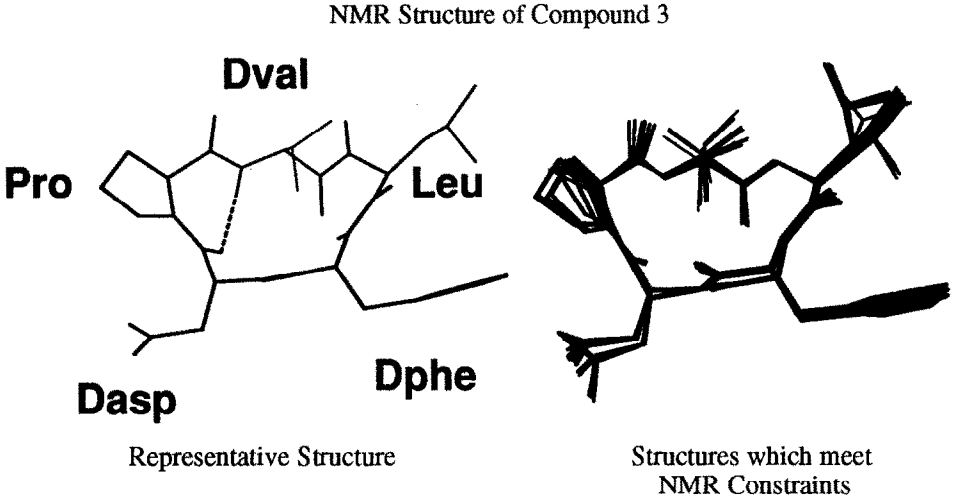

Figure 9. Compound **3** [Dphe[1]], (Right) the final 22 refined NMR structures, with backbones (N, CA, C, O) superimposed; (Left) the centroid[35] from the refined NMR structures. Note: In contrast to the DG/MD models, the sidechains are well constrained, especially the αβ-bond vector. The average mainchain RMSD between the final structures is 0.22 Å.

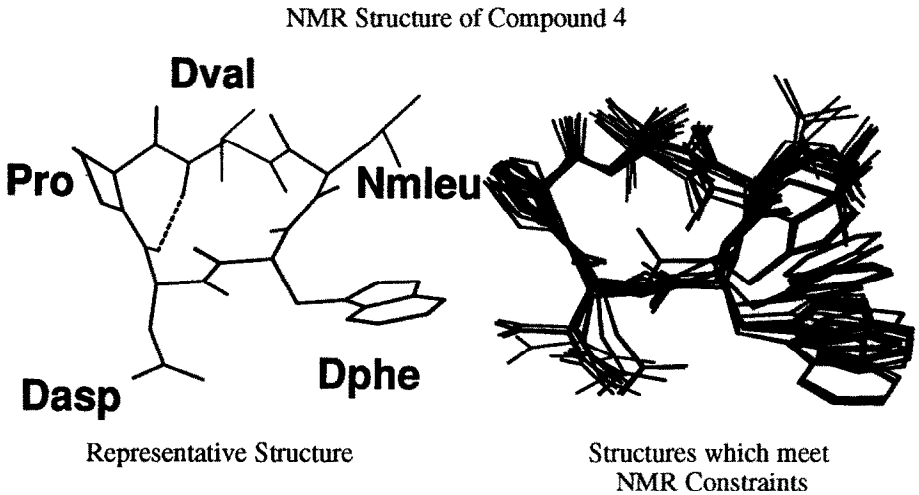

Figure 10. Compound **4** [Nmleu[5]], (Right) the final 20 refined NMR structures, with backbones (N, CA, C, O) superimposed; (Left) the centroid[35] from the refined NMR structures. Note: The conformers are not as well converged as the other 3 analogues. This probably due to the smaller number of ROE and dihedral constraints. The average mainchain RMSD between the final structures is 0.65 Å.

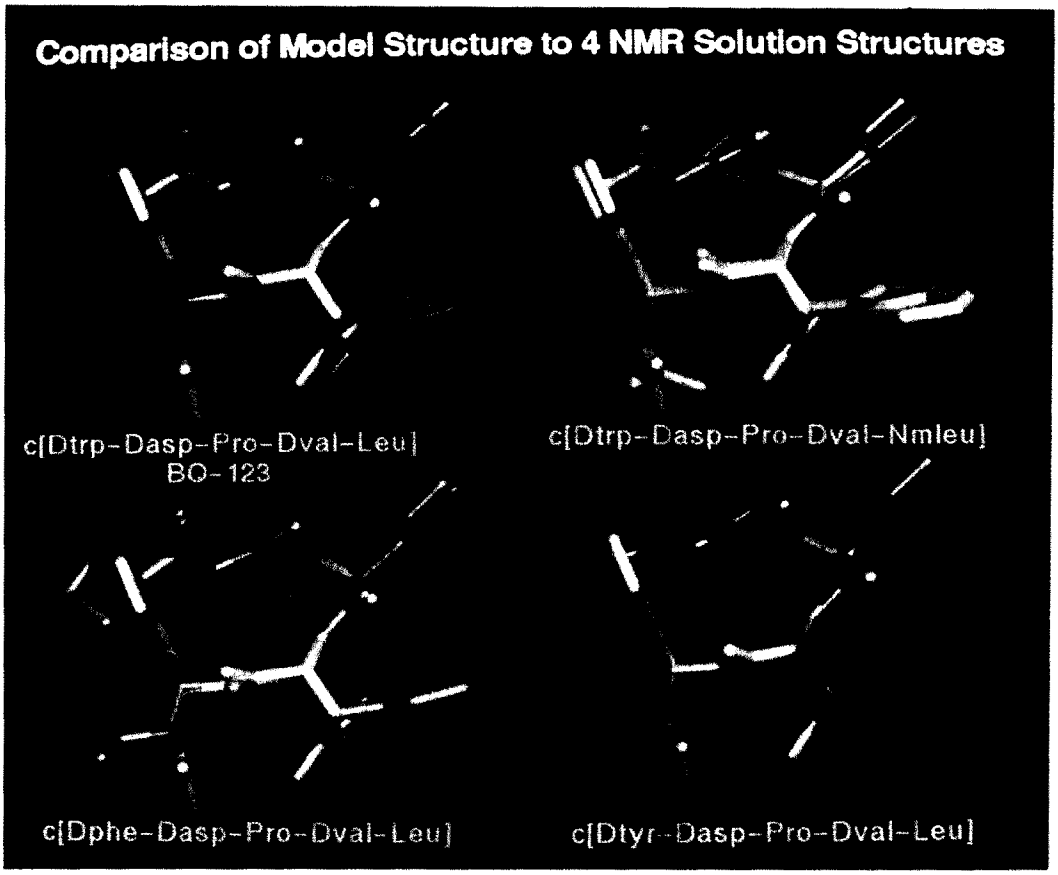

Figure 11. Superimposition of the NMR centroid backbone (N, CA, C, O) of each of the analogues on the MM/MD model of compound **4** [Nmleu^5]. (Clockwise from upper left) Compound **1** mainchain RMSD 0.35 Å, compound **2** mainchain RMSD 0.45 Å, compound **4** mainchain RMSD 0.33 Å, compound **3** mainchain RMSD 0.17 Å. Note: each of the analogues appears to adopt the same mainchain conformation as the predicted model, with compound **4** [Nmleu^5] matching its own model the best.

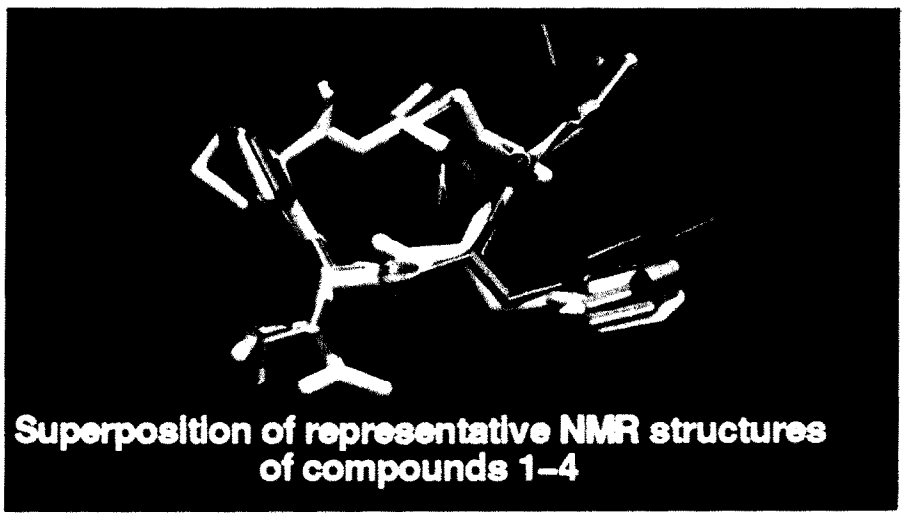

Figure 12. Backbone (N, CA, C, O) superimposition of NMR centroid structures. The average mainchain RMSD is 0.34 Å. Note: All of the analogues appear to adopt the same main chain conformation.

Table 5. Structure refinement.

Compound	Average RMSD† (Å)		RMSD with Model* (Å)	# Final Structures	Maximum Violation		Rotational Barrier§ (kcal/mol)	# Constraints	
	main chain	all atom			angle (°)	distance (Å)		distance	angle
BQ-123	0.08	0.60	0.20	4	8	0.36	10	31	4
	0.14	0.70	0.35	22	10	0.49	100	31	6
Dtyr^1	0.00	0.60	0.51	3	8	0.38	10	35	4
	0.08	0.71	0.45	36	10	0.42	100	35	6
Dphe^1	0.23	1.53	0.33	25	9	0.41	10	31	4
	0.22	0.95	0.33	22	6	0.42	100	31	6
Nmleu^5	0.65	1.35	0.17	20	10	0.41	100	21	3

†Average RMSD between final converged structures.
*RMSD between the main chain of the predicted Nmleu^5 structure and the centroid of final converged structures.
§Force constant used to calculate rotational barrier for peptides bonds.

Table 6. Comparison of ϕ,ψ of final structures.

Residue Angle	Nmleu^5 MM/MD	Nmleu^5 NMR*	BQ-123*	Dtyr^1*	Dphe^1*	Atkinson & Pelton†	Krystek et al.§ DISCOVER	Krystek et al.§ CONGEN	Reily et al.‡	Coles et al.∞
1 ϕ	138	134	123	128	131	80	81	83	84	109
ψ	47	62	37	3	41	50	27	15	29	6
2 ϕ	113	100	135	152	133	140	150	145	145	148
ψ	-96	-100	-106	-90	-119	-90	-94	-90	-128	-97
3 ϕ	-82	-79	-79	-78	-68	-75	-81	-81	-78	-74
ψ	60	69	75	68	75	85	51	40	82	82
4 ϕ	123	125	108	106	105	100	128	127	123	91
ψ	-93	-88	-137	-134	-129	-100	-126	-119	-47	-148
5 ϕ	-111	-115	-64	-68	-79	-80	-76	-104	-166	-61
ψ	58	66	65	81	67	100	107	124	100	103

*Angles from the centroid of final converged structures.
†Final values for BQ-123 from Atkinson & Pelton.[21]
§Final values for BQ-123 from Krystek *et al.*[22]
‡Final values for BQ-123 from Reily *et al.*[23]
∞Final values for BE18257B from Coles *et al.*[24]

sidechain. The first amino acid was attached to the resin with DMAP (dimethylaminopyridine) catalyzed DIC (diisopropylcarbodiimide) activation.[44] Since this acid-labile resin cleaves under even modestly acidic conditions, care was taken to ensure a basic environment at all times during the synthesis. The unreacted resin groups were capped with benzoic anhydride in pyridine/methanol before further synthesis.[47] Standard PyBOP/HOBt coupling protocols were used for the Pro, Dasp(OtBu), and Dtrp residues. Nmleu was coupled with PyBroP.[26] The peptide resin was cleaved with 1% TFA/DCM and drained into a neutralizing solution of pyridine and methanol to maintain the Dasp sidechain protection. Upon concentration, **4a** was obtained as an oil in *ca* 70% purity. Cyclization occurred in a similar manner, with yield as for **1–3**. The final product **4** was obtained after removal of the *t*-butyl ester with aqueous TFA and purification by preparative C_{18} RP-HPLC.

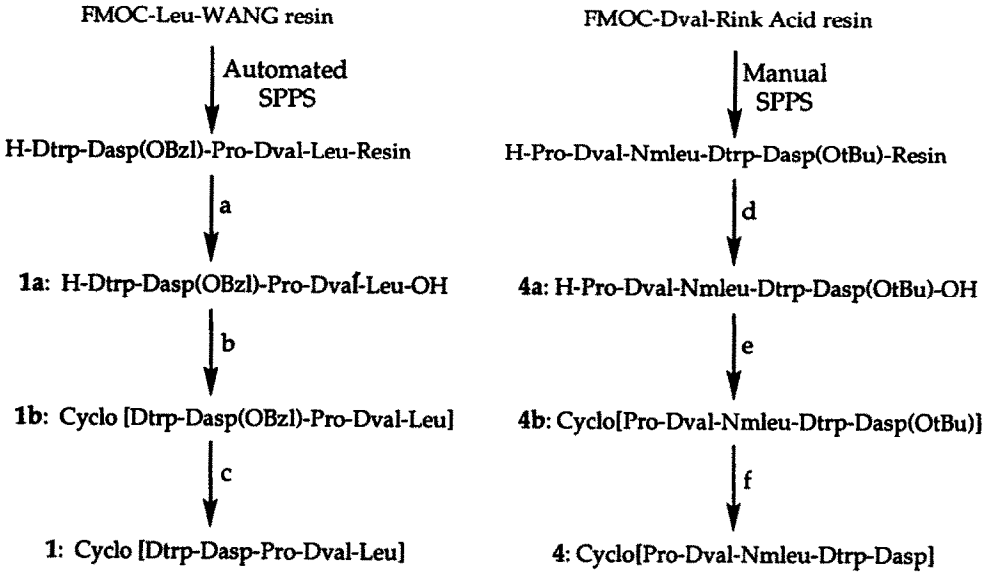

Figure 13. Scheme employed for synthesis, cleavage, and cyclization of compounds **1** and **4**. Automated solid-phase peptide synthesis: (a) 95% aqueous TFA, 2 h, room temp; (b) PyBOP, HOBt, DIEA (2.5, 2.5, 5 eq to resin), DMF, 24 h; (c) H_2, Pd/C, EtOH, HOAc, 2 h. Manual solid-phase peptide synthesis: (d) 1 % TFA/DCM, 3X2 min; (e) PyBOP, HOBt, DIEA (2.5, 2.5, 5 eq to resin), DMF, 24 h; (f) 90 % aqueous TFA 20 min, room temperature.

General

The reagents used in peptide synthesis were as follows: Rink acid-labile resin (4-(2',4'-dimethoxyphenyl-hydroxy-methyl)-phenoxy resin, 100–200 mesh, 1% cross linked with divinylbenzene) was purchased from Calbiochem (San Diego, CA), and other chemicals for peptide synthesis were purchased from Advanced Chemtech (Lexington, KY) or Novabiochem (San Diego, CA) and used as received.

The peptides were characterized by RP-HPLC, fast atom bombardment (FAB) mass spectra, and amino acid analysis (AAA). Analytical RP-HPLC chromatography was performed on a Hewlett–Packard 1090 M equipped with a diode-array detector. Preparative HPLC was performed on a Rainin HPLC system equipped with an Knauer variable wavelength detector. Gradient elution was used (A: water, 0.1% TFA, B: acetonitrile, 0.1% TFA) through Vydac C_{18} RP-HPLC columns: 4.6 mm for analytical work, 22 mm for preparative work. Analytical conditions: 0.8 mL/min flow rate, linear gradient of 5–65% buffer B in 30 min, detection at 214 and 280 nm. Preparative conditions for compounds **1**, **2** and **3**: 9.5 mL/min flow rate, linear gradient of 10–45% buffer B in 50 min, detection at 214 nm. Preparative conditions for compound **4**: 9.5 mL/min flow rate, linear gradient of 10–69% buffer B in 118 min, detection at 214 nm. FAB mass spectra were obtained in either nitrobenzyl alcohol or thioglycerol matrices at the University of California mass spectrometry facilities (Berkeley, CA), or at Mass Search (Modesto, CA). Amino acid compositions were obtained using the picotag method of Waters Associates.[48] Analyses were performed on samples hydrolyzed in vapors of constant-boiling HCl containing 1% (v/v) phenol for 22–24 h, *in vacuo*, at 110 °C prior to derivatization.

Synthesis using Wang resin

(See Figure 13) Compound **1** was prepared on ABI 431 peptide synthesizer, compounds **2** and **3** synthesized by robotic synthesizer.[49]

1a: H-Dtrp-Dasp(OBzl)-Pro-Dval-Leu-OH. The resin (300 mg, 0.14 mmol) was treated with 95% TFA (10 mL) at room temperature for 2 h, concentrated *in vacuo*, and lyophilized giving 53.3 mg of crude product. The product (R_t = 32.7 min) was obtained in ~80 % purity.

1b: Cyclic[Dtrp-Dasp(OBzl)-Pro-Dval-Leu]. Crude **1a** (35 mg, 50 μmol) was dissolved in 20 mL of DMF. PyBOP (64.3 mg, 123 μmol), 0.5M HOBT/DMF (240 μl, 120 μmol) and DIEA (42 μL, 240 μmol) were added. The solution was mixed gently for 24 h at room temperature. Cyclization was complete after 24 h (R_t = 37.9 min).

1: Cyclic[Dtrp-Dasp-Pro-Dval-Leu]. Crude **1b** was dissolved in ethanol (3 mL) and acetic acid (3 mL) and treated with palladium on charcoal (10%, 47 mg) under hydrogen at room temperature for 90 min. The product (R_t = 30.03 min) was obtained as an oil after filtration and concentration. The crude peptide was dissolved in 50% HOAc/H_2O (10 mL) and loaded onto a preparative C_{18} column. The product (> 95 % purity, R_t = 37 min) was then lyophilized giving 8.2 mg of a white fluffy powder. AAA: Trp(nd), Asp(1.07), Pro(1.10), Val(1), Leu(0.99). MS: m/z 611.4 $(MH)^+$.

2a: H-Dtyr-Dasp(OBzl)-Pro-Dval-Leu-OH. The resin (100 mg, 0.05 mmol) was treated in a similar manner to **1** giving 19 mg (R_t = 28.5 min) in > 90 % purity.

2b: Cyclic[Dtyr-Dasp(OBzl)-Pro-Dval-Leu]. Crude **2a** (4.8 mg, 20 μmol) was cyclized as in **1b**. The product had a retention time of 32.8 min.

2: Cyclic[Dtyr-Dasp-Pro-Dval-Leu] Crude **2b** was hydro-

genated and purified in a similar manner to **1b** to give 3.8 mg isolated product (> 95 % purity, R_t = 24.4 min). AAA: Tyr(1.03), Asp(1.06), Pro(1.09), Val(1), Leu(1.07). MS: m/z 588.3 $(MH)^+$.

3a: H-Dphe-Dasp(OBzl)-Pro-Dval-Leu-OH. The resin (~100 mg, 0.05 mmol) was treated in a similar manner to **1** giving 21 mg (R_t = 30.6 min) in ~90 % purity.

3b: Cyclic[Dphe-Dasp(OBzl)-Pro-Dval-Leu]. Crude **3a** (13.3 mg, 20 μmol) was cyclized as in **1b**. The product had a retention time of 37 min.

3: Cyclic[Dphe-Dasp-Pro-Dval-Leu]. Crude **3b** was hydrogenated and purified in a similar manner to **1b** to give 3.3 mg isolated product (>95 % purity, R_t = 29.3 min). AAA: Phe(1.07), Asp(1.11), Pro(1.11), Val(1), Leu(1.11). MS: m/z 572.3 $(MH)^+$.

Synthesis using Rink super acid labile resin

The linear sequence was prepared manually on Rink super acid labile resin (See Figure 13) using standard protocols.[46]

4a: H-Pro-Dval-Nmleu-Dtrp-Dasp(OtBu)-OH. The resin (650 mg, 0.15 mmol) was swollen in DCM, followed by three TFA treatments: 1 % TFA/DCM (5 mL) for 2 min and then filtered into 10 % pyridine/methanol (1 mL). The filtrates were then combined and concentrated *in vacuo* giving 294 mg of crude product, R_t = 33.9 min, in ~70 % purity.

4b: Cyclic[Dtrp-Dasp(OtBu)-Pro-Dval-Nmleu]. Crude **4a** (40 mg, 57 μmol) was dissolved in 20 mL of DMF. PyBOP (65 mg, 123 μmol), 0.5M HOBT/DMF (240 μl, 120 μmol) and DIEA (42 μL, 245 μmol) were then added. The solution was mixed gently for 24 h at room temperature and monitored by RP-HPLC. Product formation (R_t = 38.7 min) was complete after 24 h. The solvent was evaporated *in vacuo* giving 1 mL of crude product as a brown oil.

4: Cyclic[Dtrp-Dasp-Pro-Dval-Nmleu]. The crude peptide (**4b**) was treated with 90 % TFA/H_2O (2 mL) for 20 min at room temperature. The solvent was removed *in vacuo* to give crude product (R_t = 31.8 min) which was dissolved in 20 % HOAc/H_2O (10 mL) and loaded onto a C_{18} preparative column. The product fraction (R_t = 64.3 min) was lyophilized to give 0.8 mg of a white fluffy powder. The purity was > 95 %. AAA: Trp(nd), Asp(0.96), Pro(1.03), Val(1), Nmleu(nd). MS: m/z 625.4 $(MH)^+$.

Distance geometry, molecular mechanics and molecular dynamics.

Four simulations were performed for each of compounds **1–4**. They differed only in the distance geometry method used to compute the initial starting configurations.[50] With each compound, the same protocol was used for generation of molecular topology and simulation of conformational sampling. Four different methods were used to generate the starting conformations of each of the compounds:

1) Standard options available in QCPE program DGEOM,[50] a general distance geometry modeling package.
2) A modified version of DGEOM employing no distance geometry embedding, but rather using random initial Cartesian coordinates followed by minimization with the standard DGEOM error function. This method will be referred to as the RANDOM method.[51]
3) Partial metrization method[52] for improved sampling. This method will be referred to as METRIZE.
4) A modified version of DGEOM employing the standard distance geometry embedding algorithm for generation of initial Cartesian coordinates, followed by one round of conjugate gradient minimization, a round of dynamics, and finally, a second round of conjugate gradient minimization all using the standard DGEOM error function. This method will be referred to as DGDYN. (Note that these methods will be available soon in a new QCPE release of DGEOM).

For each of these methods, 500 random starting conformations were generated using DGEOM, for a total of 2000 initial conformations for each compound. In two cases (compounds **3** and **4**), the peptide bonds were allowed to float between *cis* and *trans* during the DGEOM runs. An additional set of 500 conformations of compound **3** (Dphel) was generated with all *trans* peptide bonds using the DGDYN method. Only 100 conformations of compound **5** were generated using the DGDYN protocol. No further calculations were performed on this peptide.

Each of the resulting conformations were then subjected to minimization, molecular dynamics, and further minimization using the AMBER[53] all-atom force-field implemented in the SPASMS[54] molecular mechanics and dynamics program. Unusual amino acids and molecular topologies were generated with the Prep-Link-Edit-Parm package of the AMBER 3.0A programs.[55] Topologies are available upon request. All simulations were performed in the gas phase using an infinite cutoff and a distance dependent dielectric constant (ε = 4, scee = 0.5 — the scaling factor for the 1,4 electrostatic interactions). The first and second minimizations were terminated when the gradient reached 0.001 and 0.0001 kcal/mol· Å, respectively. The molecular dynamics calculations were carried out for 6 ps (0.0015 fs timestep). The system was coupled to a temperature bath (600 K) with major stochastic collisions[56] every 500 steps and RATTLE[57] was used to hold the bond lengths constant (0.0005 Å tolerance). One simulation was performed using the same protocol, but employing a different distance dependent dielectric constant (ε = 16, scee = 2.0 — the default value) to assess the overall effect of our choice of dielectric constants in these simulations. All calculations were carried out on IBM RS-6000 models 350, 550, and 580 running AIX 3.1.5 or AIX 3.2.

NMR spectroscopy

Samples for 2D experiments were prepared as approximately 5 mM peptide in DMSO, except compound **4** which was 2 mM. TMS was used as an internal standard. All spectra were obtained at 30 °C on a Varian Unity-300.

Phase-sensitive double quantum filtered COSY[58,59] and TOCSY[30] sequences were used for spin system assignments. Phase-sensitive ROESY[31,32] experiments

with 200 ms mixing times were used for sequential assignments and evaluation of secondary structure. $^3J_{\alpha\beta}$ coupling constants were determined from a PECOSY[33] experiment. The $^3J_{N\alpha}$ coupling constants were determined from 1D spectra of 32K points.

A total of 512 t_1 increments and 2048 complex data points in t_2 were collected for each spectra. Spectral widths of 4000 Hz were used in both dimensions. The ROESY spectra were zero-filled to give final real data matrices of 2048 points in both ω_1 and ω_2. The PECOSY spectra were zero-filled to a final real data matrix of 2048 points in ω_1 and 4096 points in ω_2. All other spectra were zero-filled to give a final real data matrix of 1024 points in ω_1 and 2048 points in ω_2. The ROESY spectra had 64 acquisitions per t_1 increment, while all other spectra contain 16 acquisitions. The carrier frequency was placed at 5.0 ppm. The residual H_2O resonance was irradiated during the relaxation delay time.

Data processing was carried out with the NMR Pack software[60] on a Sun Sparc station IPC. Baseline corrections were performed as described in Basus.[61] Crosspeak intensities were determined by volume integration using the SPARKY program in NMR Pack.[60]

NMR Refinement

Distances were calculated from intensities of the 200 ms ROESY crosspeaks using the 2-spin approximation. Crosspeaks from both sides of the diagonal were integrated and a 25% error was then added to, and subtracted from, that value to provide an upper and lower bound for crosspeak intensity. Two upper distances and two lower distances were then calculated from the two crosspeaks (on either side of the diagonal) using the fixed ββ-distances for calibration. The DGEOM upper bound was set at the maximum of the two upper distances and the lower bound was set at the smaller of the two lower distances. The weakest peak seen in the spectrum had a calculated distance of approximately 3.4 Å. This overall upper distance boundary was confirmed by weak and missing intra-residue NH/CαH peaks, whose maximum distance is ~3.5 Å. The calculated lower limits were in agreement with the expected short intra-residue αβ and αN distances of approximately 2.2 Å. Our calibration method is similar to the approach described by Montelione.[62]

Dihedral constraints were determined from $^3J_{N\alpha}$ values as follows: a theoretical θ was calculated from the $^3J_{N\alpha}$ value using the equation from Pardi *et al.*[63] A window of ± 10° from calculated θ was used as the dihedral constraint. These values are listed in Table 3. This resulted in constraints for residues 2 and 4 near the *trans* region for NH/CαH. The other residues had more than one possible θ region. In order to determine the correct region, simulations were run with ROESY distance constraints and the unambiguous dihedral constraints of residues 2 and 4. The experimental dihedral ranges for residues 1 and 5 were then chosen to agree with the preliminary refined conformations containing no violations. Table 3 contains all the possible dihedral ranges for the experimental $^3J_{N\alpha}$ values, as well as the final constraints used. Dihedral constraints were applied directly to the HN-N-CA-HA dihedral angle (θ) and not translated into φ.

DGEOM[50] was used to generate 100 initial conformations with the NMR distance constraints using the RANDOM method described above. The number of distance constraints used for each analogue are shown in Table 5 and the actual constraints are available upon request. The initial DGEOM conformations were refined in three steps with minimization, molecular dynamics, and further minimization using the AMBER[53] all-atom force-field implemented in the SPASMS[54] molecular mechanics and dynamics program. The NMR distance constraints and dihedral constraints on θ (HN-N-CA-HA) and χ (N-CA-CB-CG) were included in the minimization and dynamics as flatwell potentials with harmonic boundaries.[55] All simulations were performed in the gas phase using an infinite cutoff and a distance dependent dielectric constant (ε = 4).

The initial minimization was performed on the DGEOM generated conformations with flatwell potentials of 25 kcal/mol and 50 kcal/mol for the distance and dihedral constraints, respectively, and terminated when the gradient reached 0.001 kcal/mol Å. Next, two molecular dynamics simulations were carried out. The first was for 5 ps (0.0015 fs timestep) with the system coupled to a temperature bath (300 K as described above) again using the flatwell potentials of 25 kcal/mol and 50 kcal/mol for the distance and dihedral constraints, respectively.

The second dynamics run was for 10 ps at 300 K with the flatwell potentials of 50 kcal/mol and 75 kcal/mol, respectively. Then two minimizations were performed. The first minimization was performed with flatwell potentials of 50 kcal/mol and 75 kcal/mol for the distance and dihedral constraints, respectively, and terminated when the gradient reached 0.001 kcal mol^{-1} $Å^{-1}$. The second was performed with flatwell potentials of 25 kcal/mol and 50 kcal/mol and terminated when the gradient reached 0.0001 kcal/mol Å.

Three separate sets of minimization/dynamics/-minimization refinement were carried out. The first refinement included the NMR distance constraints and the θ constraints for residues 2 and 4. The second refinement run used the θ constraints for residues 1 and 4 in addition to those of the first run. A third set of refinements was run using the increased potential on the *cis/trans* interconversion of the peptide bond. The force constant was 100 kcal/mol, which was 10 times greater than the normal value of 10 kcal/mol used in the original refinements. At this time, the χ angle constraints for residues 1 and 2 were also available and were included in this last refinement run. All other parameters remained the same. Stereospecific assignments and resulting constraints are shown in Table 5. All calculations were carried out on an IBM RS-6000 model 550, 350, or 580 running AIX 3.1.5 or AIX 3.2.

Conclusions

The results presented here demonstrate that with the combined distance geometry and molecular mechanics/dynamics protocol, it is possible to predict a low energy conformation for a cyclic pentapeptide (Nmleu^5) when the molecule is adequately constrained. Further, the well defined NMR solution structures are in agreement with the predicted conformation of Nmleu^5, confirming the MM/MD model as the actual solution conformation of all five analogues.

The main chain appears to adopt a dominant well-defined conformation, which is the same for all these analogues (Figure 12). The different IC_{50} values are probably due solely to the characteristics of the sidechains occupying the first (Dtrp) position. The IC_{50} for inhibition of ET-1 binding to ETR_A receptor of BQ-123, Dtyr^1, Dphe^1 and Nmleu^5 are shown in Table 1. It is interesting to note that compound **4**, which has an N^{α} methyl group at residue 5, has slightly different [ϕ, ψ] angles for both the Dval and the Leu (or Nmleu) residues from the other analogues. Compounds **1**, **2**, and **3** have [ϕ, ψ] angles of approximately [106, –133] for residue 4, and [–70, 70] for residue 5, while both the MM/MD model and NMR conformation of compound **4** have [ϕ, ψ] pairs of approximately [124, –90] and [–112, 62] for residues 4 and 5, respectively.

When attempting to explain activity data based on the NMR solution structures, there may be questions concerning the validity of using structures determined in DMSO at 30 °C, when binding data was acquired in aqueous buffer. In many instances this would present a problem. One such example is the cyclosporin/cyclophilin story. The solution structures of cyclosporin determined in organic solvents[36–38] have recently been shown to be very different from that of cyclosporin complexed with cyclophilin,[39–41] in aqueous solutions. In addition, the cyclophilin bound structure is very similar to an antibody bound form, which presumably reflects the aqueous solution structure.[42] Wiley and Rich have suggested that neither organic solution structures or *in vacuo* simulations are relevant to the conformation of the ligand, either in aqueous solution or bound to the receptor.[43] They propose that flexible ligands like cyclosporin undergo 'hydrophobic collapse' when dissolved in water.[43] This term is used to describe the result of molecules minimizing their exposed hydrophobic surfaces when in water by packing their hydrophobic groups together. Small flexible molecules will form new intramolecular hydrophobic interactions in aqueous solutions that are not present in organic solvents. Thus, in the case of cyclosporin and similar molecules,[43] the bioactive conformation appears to be similar to the aqueous conformation so that the organic solution structures could not be used as models for drug design.

In contrast to the cyclosporin system, there is evidence to suggest that the conformation of the peptides studied here is basically the same in aqueous solution as in DMSO. Previous work by Atkinson and Pelton[21] has shown with circular dichroism that the conformation of BQ-123 (compound **1**) is the same in either 100% H_2O or 60% acetonitrile/H_2O. In addition, work by Reily and co-workers indicates that the conformation of this molecule, as measured by ROESY spectra, was the same in either 60% acetonitrile/H_2O or neat DMSO, with only small changes in hydrophobic sidechain proximity.[23] This is not in conflict with the hydrophobic collapse theory. In this system the cyclic main chain is not flexible, but actually rigid enough to withstand hydrophobic collapse resulting in the solution structures in DMSO and H_2O being very similar. Thus it seems reasonable that the receptor-bound conformation is also close to the DMSO solution structure, the main chain scaffold being rigid and unlikely to change upon binding. Structure based design of an antagonist should now be possible with the active conformations of these molecules.

Acknowledgements

We would like to thank Sue Kaufmann and Suzy Brown for the receptor binding assays, Janice Kerr for the robot synthesis of compounds **2** and **3**, Mike Siani and Jeff Blaney for assistance with data analysis programs, Steve Cheatham at Varian for the PECOSY sequence, and Bill Sherwood, Valerie Daggett, Shauna Farr-Jones, Gerhard Wagner, Ian Campbell, and Guy Montelione for helpful discussions. We are grateful to J. Scott Dixon for implementing the partial metrization method in DGEOM and for allowing us access to this code.

References

1. Yanagisawa, M.; Kurihara, H.; Kimura, S.; Tomobe, Y.; Kabayashi, M.; Mitsui, Y.; Yazaku, Y.; Goto, K.; Masaki, T. *Nature* **1988**, *332*, 411.

2. Ihara, M.; Noguchi, K.; Saeki, T.; Fukuroda, T.; Tsuchida, S.; Kimura, S.; Fukami, T.; Ishikawa, K.; Nishikibe, M.; Yano, M. *Life Sci.* **1991**, *50*, 247–255.

3. Clozel, M.; Gray, G.; Breu, V.; Loffler, B.-M.; Osterwalder, R. *Biochem. Biophys. Res. Commun.* **1992**, *186*, 867–873.

4. Ihara, M.; Fukuroda, T.; Saeki, T.; Nishikibe, M.; Kojiri, K.; Suda, H.; Yano, M. *Biochem. Biophys. Res. Commun.* **1991**, *178*, 132–137.

5. Ishikawa, K.; Fukami, T.; Hayama, T.; Niiyama, K.; Nagase, T.; Mase, T.; Fujita, K.; Kumagai, U.; Urakawa, Y.; Kimura, S.; Ihara, M.; Yano, M. Twelfth American Peptide Symposium, Cambridge, MA, 1991.

6. Ishikawa, K.; Fukami, T.; Nagase, T.; Fujita, K.; Hayama, T.; Niiyama, K.; Mase, T.; Ihara, M.; Yano, M. *J. Med. Chem.* **1992**, *35*, 2139–2142.

7. Miyata, S.; Fukami, N.; Neya, M.; Takase, S.; Kiyoto, S. *J. Antibiot.* **1992**, *45*, 788–791.

8. Hemmi, K.; Neya, M.; Fukami, N.; Hashimoto, M.; Tanaka, H.; Kayakiri, N. Eur. Pat. Appl. 0457195A2, published November 21, 1991.

9. Ishikawa, K.; Fukami, T.; Hayama, T.; Niiyama, K.; Nagase, T.; Mase, T.; Fujita, K.; Ihara, M.; Ikemoto, F.; Yano, M. Eur. Pat. Appl. 0460679A2, published December 11, 1991.

10. Doherty, A. M.; Cody, W. L.; DePue, P. L.; He, J. X.; Waite, L. A.; Leonard, D. M.; Leitz, N. L.; Dudley, D. T.; Rapundalo, S. T.; Hingorani, G. P.; Haleen, S. J.; LaDouceur, D. M.; Hill, K. E.; Flynn, M. A.; Reynolds, E. E. *J. Med. Chem.* **1993**, *36*, 2585–2594.

11. Cody, W. L.; Doherty, A. M.; He, J. X.; DePue, P. L.; Rapundalo, S. T.; Hingorani, G. A.; Major, T. C.; Panek, R. L.; Dudley, D. T.; Haleen, S. J.; LaDouceur, D.; Hill, K. E.; Flynn, M. A.; Reynolds, E. E. *J. Med. Chem.* **1992**, *35*, 3301–3303.

12. Doherty, A. M.; Cody, W. L.; He, X.; DePue, P. L.; Leonard, D. M.; Dudley, D. T.; Rapundalo, S. T.; Hingorani, G. P.; Panek, R. L.; Major, T. C.; Hill, K. E.; Flynn, M. A.; Reynolds, E. E. 203rd National Meeting of the American Chemical Society, San Francisco, April 1992.

13. Doherty, A. M.; Cody, W. L.; Leitz, N. L.; DePue, P. L.; Taylor, M. D.; Rapundalo, S. T.; Hingorani, G. P.; Major, T. C.; Panek, R. L.; Taylor, D. G. *J. Cardiovasc. Pharmacol.* **1991**, *17 (Suppl. 7)*, S59–S61.

14. Spellmeyer, D. C.; Brown, S.; Stauber, G. S.; Geysen, H. M.; Valerio, R. *BioMed. Chem. Lett.* **1993**, *3*, 519–524.

15. Spellmeyer, D. C.; Brown, S.; Stauber, G. S.; Geysen, H. M.; Valerio, R. *BioMed. Chem. Lett.* **1993**, *3*, 1253–1256.

16. Oohata, N.; Nishikawa, M.; Kiyoto, S.; Takase, S.; Hemmi, K.; Murai, H.; Okuhara. M. Eur. Pat. Appl. 0405421A2, published January 2, 1991.

17. Lam, Y. K. T.; Hensens, O. D.; Liesch, J. M.; Zink, D. L.; Huang, L.; Williams, Jr, D. L.; Genilloud, O. R. Eur. Pat. Appl. 0496452A1, published July 29, 1992.

18. Fujimoto, M.; Mihara, S.; Nakajima, S.; Ueda, M.; Nakamura, M.; Sakurai, K. *FEBS Lett.* **1992**, *305*, 41–44.

19. Burri, K.; Clozel, M.; Fischil, W.; Hirth, G.; Löffler, B. M.; Ramuz, H. Eur. Pat. Appl. 0510526A1, published October 28, 1992.

20. Clozel, M.; Breu, V.; Burri, K.; Cassal, J.-M.; Fischil, W.; Gray, G. A.; Hirth, G.; Löffler, B. M.; Muller, M.; Neidhart, W; Ramuz, H. *Nature* **1993**, *365*, 759–761.

21. Atkinson, R. A.; Pelton, J. T. *FEBS Lett.* **1992**, *296*, 1–6.

22. Krystek, S. R.; Bassolino, D. A.; Bruccoleri, R. E.; Hunt, J. T.; Porubcan, M. A.; Wandler, C. A.; Anderson, N. H. *FEBS Lett.* **1992**, *299*, 255–261.

23. Reily, M. D.; Thanabal, V.; Omecinsky, D. O.; Dunbar, J. B.; Doherty, A. M.; DePue, P. L. *FEBS Lett.* **1992**, *300*, 136–140.

24. Coles, M.; Sowemimo, V.; Scanlon, D.; Munro, S. L. A.; Craik, D. J. *J. Med. Chem.* **1993**, *36*, 2658–2665.

25. Frerot, E.; Coste, J.; Panataloni, A.; DuFour, N.; Jouin, P. *Tetrahedron* **1991**, *47*, 259–270.

26. Castro, B.; Coste, J.; DuFour, N.; Pantaloni, A. In *Peptides: Chemistry, Structure, and Biology: Proceedings of the Eleventh American Peptide Symposium*, pp. 900–901, Rivier, J. E.; Marshall, G. M., Eds.; Escom: Leiden, The Netherlands 1990.

27. Peishoff, C. E.; Dixon, J. S.; Kopple, K. D. *Biopolymers* **1990**, *30*, 45–56.

28. Kollman, P. A. personal communication.

29. Wuthrich, K.; Wider, G.; Wagner, G.; Braun, W. *J. Mol. Biol.* **1982**, *155*, 311–319.

30. Bothner-By, A. A.; Stephens, R. L.; Lee, J.; Warren, C. D.; Jeanloz, R.L., *J. Am. Chem. Soc.***1984**, *106*, 811–813.

31. Bax, A.; Davis, D. G. *J. Magn. Res.* **1985**, *63*, 207–213.

32. Davis, D. G.; Bax, A. *J. Magn. Res.* **1985**, *65*, 355–360.

33. Mueller, L. *J. Magn. Res.* **1987**, *7*, 191–196.

34. Basus, V. J. *Meth. Enzymol.* **1989**, *17*, 132–149.

35. The centroid of N structures is determined by making an N x N matrix of RMSD values, and calculating the N-dimensional center of geometry of the N structures. The centroid is the conformer closest to the center of geometry, which is equivalent to the conformer closest to the average, or the 'mean' structure.

36. Kessler, H.; Loosli, H.-R.; Oschkinat, H. *Helv. Chim. Acta* **1985**, *68*, 661–681.

37. Loosli, H.-R.; Kessler, H.; Oschkinat, H.; Weber, H.-P.; Petcher, T. J.; Widmer, A. *Helv. Chim. Acta* **1985**, *68*, 682–704.

38. Kessler, H.; Gehrke, M.; Lantz, J.; Kock, M.; Seebach, D.; Thaler, A. *Biochem. Pharmacol*, **1990**, *40*, 169–173, *erratum* 2185–2186.

39. Fesick, S. W.; Gampe, R. T.; Holzman, T. F.; Egan, D. A.; Edalji, R.; Luly, J. R.; Simmer, R.; Helfrich, R.; Kishore, V.; Rich, D. H. *Science* **1990**, *250*, 1406–1409.

40. Fesick, S. W.; Gampe, R. T.; Eaton, H. L.; Gemmecker, G.; Olejniczak, E. T.; Neri, P.; Holzman, T. F.; Egan, D. A.; Edalji, R.; Simmer, R.; Helfrich, R.; Hochlowski, J.; Jackson, M. *Biochemistry* **1991**, *30*, 6574–6583.

41. Weber, C.; Wider, G.; von Freyberg, B.; Traber, R.; Braun, W.; Widmer, H.; Wuthrich, K. *Biochemistry* **1991**, *30*, 6563–6574.

42. Altschuh, D.; Vix, O.; Rees, R.; Thierry, J.-C. *Science*, **1992**, *256*, 92–94.

43. Wiley, R. A.; Rich, D. H. *Medicinal Research Reviews* **1993**, *13*, 327–384.

44. Wang, S.-S. *J. Am. Chem. Soc.* **1973**, *95*, 1328–1333.

45. Note: compound **1** was prepared on an ABI 431, compounds **2** and **3** were prepared robotically.[49]

46. Rink, H. *Tetrahedron Lett.* **1987**, *28*, 3787–3782.

47. See NovaBiochem (La Jolla, CA 92039) catalog, 1992–3, p. 275.

48. Bidlingmeyer, B. A.; Cohen, S. A.; Tarvin, T. L. *J. Chromatogr* **1984**, *336*, 93–104.

49. Zuckermann, R.; Kerr, J.; Siani, M.; Banville, S.; Santi, D. V. *Proc. Natl. Acad. Sci. USA* **1992**, *89*, 4505–4509.

50. DGEOM: Blaney, J. M.; Crippen, G. M.; Dearing, A.; Scott Dixon, J.; 1984–1991. Available from the Quantum Chemistry Program Exchange, Bloomington, IN.

51. This program has been modified to include a molecular dynamics step after the embedding has been completed. This results in improved sampling of the distance geometry method. The standard options for DGEOM were used for generation of the conformations. Bonds were allowed to be eclipsed, and the dynamics was run for 2000 timesteps (Δt = 0.02, T=200).

52. Kuszewski, J.; Nilges, M.; Bruenger, A. T. *J. Biomolecular NMR* **1992**, *2*, 33–56.

53. Weiner, S. J.; Kollman, P. A.; Nguyen, D. T.; Case, D. A. *J. Comput. Chem.* **1986**, *7*, 230–252.

54. SPASMS: Spellmeyer, D. C.; Swope, W. C.; Evensen, E.-R.; Ferguson, D. M. 1992. Available from Department of Pharmaceutical Chemistry, University of California, San Francisco, CA 94143.

55. AMBER 3.0A: Singh, U. C.; Weiner, P. K.; Caldwell, J.; Kollman, P. A., 1989. Available from Department of Pharmaceutical Chemistry, University of California, San Francisco, CA 94143.

56. Andersen, H. C. *J. Chem. Phys.* **1980**, *72*, 2384.

57. Andersen, H. C. *J. Comput. Phys.* **1983**, *52*, 24.

58. Marion, D.; Wüthrich, K. *Biochem. Biophys. Res. Commun.* **1983**, *113*, 967–974.

59. Rance, M.; Sorensen, O. W.; Bodenhausen, G.; Wagner, G.; Ernst, R. R.; Wüthrich, K. *Biochem. Biophys. Res. Commun.* **1983**, *117*, 479–485.

60. NMR Pack: Day, M.; Kneller, D.; Kuntz, I. D. 1993. Available from Department of Pharmaceutical Chemistry, University of California, San Francisco, CA 94143.

61. Basus, V. J.; Billeter, M.; Love, R. A.; Stroud, R. M.; Kuntz, I. D. *Biochemistry*, **1988**, *27*, 2763–2771.

62. Montelione, G. T.; Wuthrich, K.; Burgess, A. W.; Nice, E. C.; Wagner, G.; Gibson, K. D.; Scheraga, H. A. *Biochemistry* **1992** *31*, 236–249.

63. Pardi, A. M.; Billeter, M.; Wüthrich, K. *J. Mol. Biol.* **1984**, *180*, 741–751.

(*Received* 15 *November* 1993; *accepted* 4 *February* 1994)